*J. Fluid Mech.* (2021), *vol*. 922, R5, doi:10.1017/jfm.2021.562

# Optimal swimmers can be pullers, pushers or neutral depending on the shape

**Abdallah Daddi-Moussa-Ider**[1], **Babak Nasouri**[2], **Andrej Vilfan**[2,3],† **and Ramin Golestanian**[2,4]

[1]Institut für Theoretische Physik II: Weiche Materie, Heinrich-Heine-Universität Düsseldorf, 40225 Düsseldorf, Germany

[2]Max Planck Institute for Dynamics and Self-Organization (MPIDS), 37077 Göttingen, Germany

[3]Jožef Stefan Institute, 1000 Ljubljana, Slovenia

[4]Rudolf Peierls Centre for Theoretical Physics, University of Oxford, Oxford OX1 3PU, UK

(Received 28 April 2021; revised 31 May 2021; accepted 18 June 2021)

The ability of microswimmers to deploy optimal propulsion strategies is of paramount importance for their locomotory performance and survival at low Reynolds numbers. Although for perfectly spherical swimmers minimum dissipation requires a neutral-type swimming, any departure from the spherical shape may lead the swimmer to adopt a new propulsion strategy, namely those of puller- or pusher-type swimming. In this study, by using the minimum dissipation theorem for microswimmers, we determine the flow field of an optimal nearly spherical swimmer, and show that indeed depending on the shape profile, the optimal swimmer can be a puller, pusher or neutral. Using an asymptotic approach, we find that amongst all the modes of the shape function, only the third mode determines, to leading order, the swimming type of the optimal swimmer.

**Key words:** propulsion

## 1. Introduction

An active particle (or microswimmer), be it a living cell or a synthetic swimmer, converts the internal or ambient free energy into work as it moves through a viscous fluid (Lauga & Powers 2009; Bechinger *et al.* 2016; Gompper *et al.* 2020). From a broad hydrodynamic perspective, the physics behind the propulsion of an active swimmer can be divided into two parts: the inner problem, which concerns the generation of the propulsive thrust, and the outer problem, which focuses on how swimmers interact with their neighbouring environment through altering their surrounding fluid. While in the former accounting for the details of the mechanism behind the impetus of each specific swimmer is essential

† Email address for correspondence: andrej.vilfan@ds.mpg.de

(for example through cilia (Blake & Sleigh 1974) or a phoretic mechanism (Golestanian, Liverpool & Ajdari 2005; Nasouri & Golestanian 2020)), in the latter, one can use a generic approach to describe the flow field induced by the swimmer (Kim & Karrila 1991; Lauga & Michelin 2016; Nasouri & Elfring 2018). Specifically for self-propelling axisymmetric swimmers, this generic approach classifies the swimmers into three groups of pushers, pullers and neutrals, often referred to as the microswimming types (Underhill, Hernandez-Ortiz & Graham 2008; Lauga & Powers 2009). This categorization, which stems from the far-field description of the motion of a particle in a viscous fluid, relies on the fact that self-propulsion is force- and torque-free, and so the leading-order flow field induced by an active swimmer can be solely described by a symmetric force dipole, i.e. stresslet (Batchelor 1970). Based on the strength of this force dipole, a swimmer is a puller when it generates the impetus from its front end, a pusher when the thrust originates from the rear end and is neutral when this strength is zero. Examples of pusher-type microswimmers include *Escherichia coli* bacteria that use bundles of rotating helical filaments in their rear (Berke *et al.* 2008), or sperm cells that propel themselves by propagating a wave along a flexible flagellum. An example of puller-type microswimmers is *Chlamydomonas reinhardtii* that pulls in the fluid in front of it with a pair of flagella beating in a breaststroke-like fashion (Kantsler *et al.* 2013). *Volvox*, a multicellular colony of green algae, is a neutral swimmer (Drescher *et al.* 2009; Pedley, Brumley & Goldstein 2016), whereas *Paramecium* is a weak pusher (Zhang *et al.* 2015).

Swimmers of different type behave differently when interacting with their surroundings. For instance, unlike puller-like swimmers, pushers can be hydrodynamically trapped by nearby obstacles or other pusher swimmers (Berke *et al.* 2008; Spagnolie *et al.* 2015; Daddi-Moussa-Ider *et al.* 2018; Sprenger *et al.* 2020). The stresslet further determines the intensity of fluid stirring in suspensions of swimmers (Lin, Thiffeault & Childress 2011). Although the effect of swimming type on the interaction of each swimmer with other swimmers/boundaries has been well explored, their energetic implications are yet to be fully understood. For surface-driven spherical swimmers, it has been shown that the viscous dissipation of neutral swimmers is minimal compared with that of pushers and pullers, and so neutral swimmers are often considered as the optimal type (Michelin & Lauga 2010). However, the innate question of whether this statement holds when the swimmer does not possess a perfect spherical shape remains largely unanswered. This is the question we address in this study.

The question of energetic efficiency and optimal propulsion, i.e. minimizing the dissipation while maintaining the swimming speed or equivalently maximizing the swimming speed while maintaining the dissipation, is a long-standing problem. Earlier theoretical works focused on the optimal locomotion of flagellated micro-organisms (Pironneau & Katz 1974; Lighthill 1975). In particular, the optimal shape of a periodically actuated planar flagellum deforming via a travelling wave has been derived computationally (Lauga & Eloy 2013), and shown to agree well with the waveform assumed by sperm cells of marine organisms. The optimal swimming strokes and self-propulsion efficiencies of spherical and cylindrical bodies undergoing small deformation with respect to a reference shape has also been investigated (Shapere & Wilczek 1987, 1989). Further studies considered the full optimization problem for simple mechanically actuated model microswimmers (Alouges, DeSimone & Lefebvre 2007; Nasouri, Vilfan & Golestanian 2019).

Generally, the quest for the optimal propulsion strategy requires both the solution of the inner and the outer problems. Swimming efficiency of ciliated microswimmers can be directly determined numerically (Ito, Omori & Ishikawa 2019; Omori, Ito & Ishikawa 2020), but it is more common to use a coarse-grained approach, namely to separately

calculate the dissipation in the propulsive layer and then replace this layer with an effective slip velocity when determining the external flow (Keller & Wu 1977; Sabass & Seifert 2010; Osterman & Vilfan 2011; Vilfan 2012). A fundamental limit on swimming efficiency can be obtained by finding the slip profile that minimizes the external dissipation for a given swimming speed. For spherical swimmers, by using the classical squirmer model of Lighthill (1952) and Blake (1971), one can show that the contribution of the second mode of squirming (which characterizes the stresslet) to the dissipated power can only be positive. Because the swimming speed for spherical squirmers is independent of this second mode, we can conclude that minimizing the dissipation requires the second mode to be zero, thereby making the optimal swimmer a neutral one (Blake 1973). However, such a simple decomposition of contributions cannot be achieved for non-spherical swimmers, and so the correlation between the dipole coefficient and the dissipation is not clearly known. Recently, using the boundary element method and numerical optimization, Guo *et al.* (2021) showed on some example shapes that when the swimmer body is not front–aft symmetric, pushers or pullers can be more efficient than neutral swimmers. In this study, we systematically investigate the relation between the stresslet and the shape of nearly spherical optimal swimmers. By employing the recently derived minimum dissipation theorem (Nasouri, Vilfan & Golestanian 2021), we circumvent the nonlinear optimization problem and arrive at the flow field for the optimal swimmer using the flow fields of two auxiliary passive problems. We remarkably find that the stresslet of an optimal swimmer is solely a function of the third Legendre mode describing the shape of the swimmer, and so depending on the value (or sign) of this mode, the optimal swimmer can be a pusher, puller or neutral.

## 2. The problem statement

In this study, our aim is to determine whether an optimal nearly spherical swimmer is a puller, pusher or neutral. To this end, we consider a swimming body of axisymmetric shape moving with a steady velocity $V_A \boldsymbol{e}_z$, where $\boldsymbol{e}_z$ is a unit vector representing the axis of symmetry. We parametrize the surface of the swimming object in axisymmetric spherical coordinates by

$$r(\theta) = a\left[1 + \sum_{\ell=1}^{\infty} \alpha_\ell P_\ell(\cos\theta)\right], \tag{2.1}$$

where $a$ denotes the radius of the undeformed sphere, $\theta$ represents the polar angle with respect to $\boldsymbol{e}_z$ and $P_\ell$ is the Legendre polynomial of degree $\ell$ (see figure 1). We assume $\alpha_\ell \ll 1$, thus the particle possesses a nearly spherical shape. Note that because the first mode merely implies body translation and does not indicate any departure from the spherical shape, we set $\alpha_1 = 0$.

At the small scales of microswimmers, viscous forces dominate inertial forces, and the flow is governed by the Stokes equations $\nabla \cdot \boldsymbol{\sigma} = \boldsymbol{0}$ and $\nabla \cdot \boldsymbol{v} = 0$ with $\boldsymbol{v}$ denoting the flow field, $\boldsymbol{\sigma} = -p\boldsymbol{I} + \mu(\nabla \boldsymbol{v} + \nabla \boldsymbol{v}^\top)$ the stress field and $p$ the pressure field. The swimmer is surface-driven and its active mechanism induces an effective tangential slip-velocity $\boldsymbol{v}^s$ on its surface, which imposes the boundary condition on the fluid velocity in the co-moving frame $\boldsymbol{v} = \boldsymbol{v}^s$. The slip profile determines the swimming velocity $V_A$ through a relationship that can be derived from the Lorentz reciprocal theorem (Stone & Samuel 1996). The dissipated power is given by $P = -\int \boldsymbol{v}^s \cdot \boldsymbol{\sigma} \cdot \boldsymbol{n}\, \mathrm{d}S$. We consider the swimmer to be optimal, thus this slip profile minimizes the viscous dissipation $P$, while maintaining the swimming speed $V_A$.

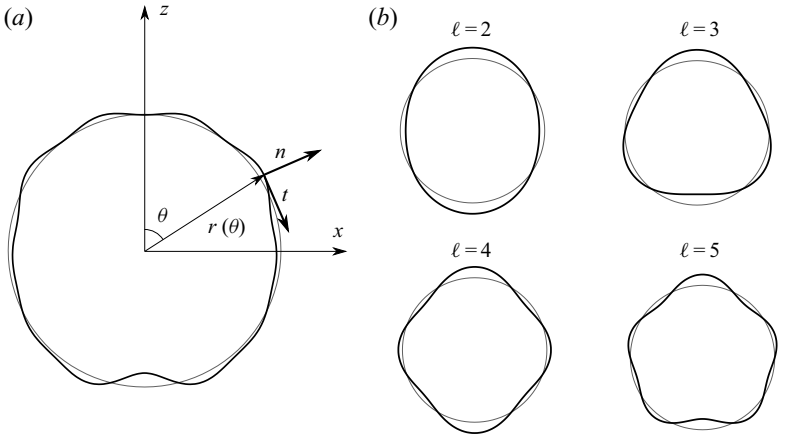


Figure 1. (*a*) Schematic of the nearly spherical swimmer described in (2.1). (*b*) The isolated contribution of the first four modes in the shape function. Black lines show the perturbed shape and the grey lines illustrate the reference unperturbed sphere.

We should note that the present analytical description of microswimmers applies exclusively to non-deformable active swimmers of nearly spherical shape. Prime examples of these swimmers include a broad class of ciliated microorganisms or synthetic microswimmers that achieve locomotion via a thin slip layer (e.g. self-phoretic mechanisms).

As discussed earlier, the far-field flow generated by the force- and torque-free motion of a microswimmer has the form (to the leading order) $\boldsymbol{v}(\boldsymbol{x}) = -(3/(8\pi\mu))(\boldsymbol{x}\cdot\boldsymbol{S}\cdot\boldsymbol{x})\,\boldsymbol{x}/r^5$ and is characterized by the stresslet $\boldsymbol{S}$. Here, because the motion is axisymmetric, the stresslet takes the simple form of

$$\boldsymbol{S} = 8\pi\mu a^2 V_A\,\beta\left(\boldsymbol{e}_z\boldsymbol{e}_z - \tfrac{1}{3}\boldsymbol{I}\right), \tag{2.2}$$

where $\beta$ is the dimensionless dipole coefficient (Batchelor 1970; Nasouri & Elfring 2018). Under this definition, the sign of $\beta$ determines the swimming type such that $\beta < 0$ holds for pushers, $\beta > 0$ for pullers and $\beta = 0$ indicates neutral swimming. Thus, to determine the swimming type of an optimal nearly spherical swimmer, we need to find the relation between $\beta$ and $\alpha_\ell$.

Conventionally, finding the flow field surrounding an optimal swimmer requires extensive optimization schemes, which are often implemented by means of computational tools. Here, we alternatively apply a fundamental theorem that sets the lower bound on the energy dissipation of a self-propelled active microswimmer of arbitrary shape (Nasouri *et al.* 2021). It states that the motion of an active swimmer with minimal dissipation can be conveniently expressed as a linear superposition of two passive bodies of the same shape satisfying no-slip and perfect-slip boundary conditions at their surfaces, respectively. This theorem relies on the fact that perfect-slip bodies require the least dissipation for motion, which suggests that a swimmer with a similar slip profile will be more efficient. A superposition with the no-slip problem is needed to obtain a force-free flow around an active swimmer (see Nasouri *et al.* (2021) for the details of the derivation). Specifically, defining $\boldsymbol{v}_A$ as the flow field induced by the motion of the optimal swimmer, this theorem dictates

$$\boldsymbol{v}_A = \boldsymbol{v}_{PS} - \boldsymbol{v}_{NS}, \tag{2.3}$$

where $\boldsymbol{v}_{PS}$ is the flow field owing to the motion of a passive perfect-slip body of the same shape translating with speed $V_{PS} = [R_{NS}/(R_{NS} - R_{PS})]V_A$, and $\boldsymbol{v}_{NS}$ is the flow field of its no-slip counterpart moving with speed $V_{NS} = [R_{PS}/(R_{NS} - R_{PS})]V_A$, with $R_{NS}$ and $R_{PS}$ being the translational drag coefficients for the no-slip and the perfect-slip body, respectively.

Accordingly, by means of this theorem, the optimization problem is reduced to finding the flow fields of two passive systems (henceforth referred to using 'PS' and 'NS') and their corresponding drag coefficients. Following an asymptotic approach, we will prove that the dipole coefficient takes a particularly simple expression and can solely be expressed in terms of the third Legendre mode as

$$\beta = \tfrac{27}{14}\,\alpha_3. \tag{2.4}$$

Based on this, the nearly spherical optimal swimmer is classified as a pusher when $\alpha_3 < 0$, puller when $\alpha_3 > 0$ and neutral if $\alpha_3 = 0$.

## 3. Solution of the passive problem

As discussed earlier, to find the flow field of the optimal active swimmer, we only need to determine the flow fields around a passive body of the same shape, once with a no-slip and once with a perfect-slip boundary condition.

Recalling that the particle is nearly spherical (i.e. $\alpha_\ell \ll 1$), we use an asymptotic approach to find the flow fields, and expand all entities in terms of surface modes. At the zeroth order (denoted by '(0)'), we recover the flow fields arising from the passive motion of a spherical particle with no-slip and perfect-slip boundary conditions. The first-order correction (denoted by '(1)') will then arise from the surface departure from the spherical shape, and so, based on the linearity of the field equations, must be a linear superposition of the surface modes, e.g. $\boldsymbol{v} = \boldsymbol{v}^{(0)} + \sum_\ell \alpha_\ell \boldsymbol{v}_\ell^{(1)}$. In what follows, we find the zeroth- and first-order flow fields for both the NS and PS problems by applying the Lamb's solution at each order separately.

We should also account for the correction to the surface normal vector at the first order. At the zeroth order we have $\boldsymbol{n}^{(0)} = \boldsymbol{e}_r$, and the departure from spherical shape leads to $\boldsymbol{n}^{(1)} = -\sum_\ell \alpha_\ell P_\ell^1(\cos\theta)\,\boldsymbol{e}_\theta$, where $P_\ell^1(\cos\theta) = \mathrm{d}P_\ell(\cos\theta)/\mathrm{d}\theta$ is the associate Legendre polynomial of the first order. The tangent vector is given by $\boldsymbol{t}^{(0)} = \boldsymbol{e}_\theta$ and $\boldsymbol{t}^{(1)} = \sum_\ell \alpha_\ell P_\ell^1(\cos\theta)\,\boldsymbol{e}_r$.

### 3.1. *No-slip problem*

The solution for the flow past a nearly spherical body with a no-slip boundary is discussed by Happel & Brenner (1983). In the following, we derive the flow field in a form that will be convenient for the solution of the active problem in the next section. Owing to the linearity of the problem, we only need to solve the flow field for a single mode of surface deformation (e.g. $\alpha_\ell$), and the complete solution will be achieved by linear superposition of all modes.

In the co-moving frame of reference, the no-slip boundary condition requires vanishing velocities at the deformed surface of the object such that

$$\boldsymbol{v}_{NS} = \boldsymbol{0} \quad \text{at } r(\theta) = a\,[1 + \alpha_\ell P_\ell(\cos\theta)]\,. \tag{3.1}$$

This condition can be expanded perturbatively to linear order in $\alpha_\ell$ as

$$\boldsymbol{v}^{(0)} + \alpha_\ell \left( \boldsymbol{v}^{(1)} + a \frac{\partial \boldsymbol{v}^{(0)}}{\partial r} P_\ell(\cos\theta) \right) \Bigg|_{r=a} = \boldsymbol{0}. \tag{3.2}$$

To find the Stokes flow that satisfies the above boundary condition, along with the condition $\boldsymbol{v} = -V_{NS}\,\boldsymbol{e}_z$ at $r \to \infty$, we use Lamb's general solution in spherical coordinates as an ansatz (Happel & Brenner 1983). For axisymmetric problems, this solution simplifies to

$$\frac{v_r}{V_{NS}} = -\cos\theta + \sum_{n=1}^{\infty} \frac{n+1}{2} \left( nA_n - 2B_n \left(\frac{a}{r}\right)^2 \right) \left(\frac{a}{r}\right)^n P_n(\cos\theta), \tag{3.3a}$$

$$\frac{v_\theta}{V_{NS}} = \sin\theta + \sum_{n=1}^{\infty} \left( -\frac{n-2}{2} A_n + B_n \left(\frac{a}{r}\right)^2 \right) \left(\frac{a}{r}\right)^n P_n^1(\cos\theta), \tag{3.3b}$$

where $A_n$ and $B_n$ are series coefficients that must be determined from the boundary conditions.

The solution for the zeroth-order problem corresponding to an undeformed sphere can readily be obtained by imposing $v_r^{(0)} = 0$ and $v_\theta^{(0)} = 0$ at $r = a$. This leads us to $A_1^{(0)} = 3/2$, $B_1^{(0)} = 1/4$ and $A_n^{(0)} = B_n^{(0)} = 0$ for $n \geqslant 2$. The zeroth-order flow field

$$\frac{v_r^{(0)}}{V_{NS}} = -\frac{1}{2}\left(2 - \frac{3a}{r} + \frac{a^3}{r^3}\right)\cos\theta, \quad \frac{v_\theta^{(0)}}{V_{NS}} = \frac{1}{4}\left(4 - \frac{3a}{r} - \frac{a^3}{r^3}\right)\sin\theta, \tag{3.4a,b}$$

represents the well-known flow past a no-slip sphere (Happel & Brenner 1983).

The boundary condition for the first-order problem (3.2) then reads $\boldsymbol{v}^{(1)} = -a(\partial \boldsymbol{v}^{(0)}/\partial r)\, P_\ell(\cos\theta)$ at $r = a$. By noting that $\partial v_r^{(0)}/\partial r = 0$ at $r = a$, we find upon using appropriate orthogonality relations that only the series coefficients of order $n = \ell \pm 1$ have non-zero values. Specifically, we find $A_{\ell-1}^{(1)} = -A_{\ell+1}^{(1)} = -(3/2)/(2\ell+1)$, $B_{\ell-1}^{(1)} = -(3/4)(\ell-1)/(2\ell+1)$ and $B_{\ell+1}^{(1)} = (3/4)(\ell+1)/(2\ell+1)$. The first-order correction to the flow can be evaluated by inserting these coefficients into the generic solution given in (3.3). Examples of flow patterns for the first three deformation modes are shown in figure 2(*a,d,g*).

The drag force exerted on an object is always determined by the force monopole as $F_D = -4\pi\mu a A_1 V_{NS}$. Accordingly, the translational drag coefficient for an approximate sphere only depends on the zeroth and second Legendre modes and can be written as (Happel & Brenner 1983)

$$\frac{R_{NS}}{6\pi\mu a} = 1 - \frac{1}{5}\alpha_2. \tag{3.5}$$

### 3.2. *Perfect-slip problem*

For the perfect-slip boundary condition, the impermeability and vanishing tangential stress need to be satisfied at the surface of the approximate sphere,

$$\boldsymbol{v}_{PS} \cdot \boldsymbol{n} = 0 \quad \text{and} \quad \boldsymbol{t} \cdot \boldsymbol{\sigma}_{PS} \cdot \boldsymbol{n} = 0 \quad \text{at } r(\theta) = a\left[1 + \alpha_\ell P_\ell(\cos\theta)\right]. \tag{3.6a,b}$$

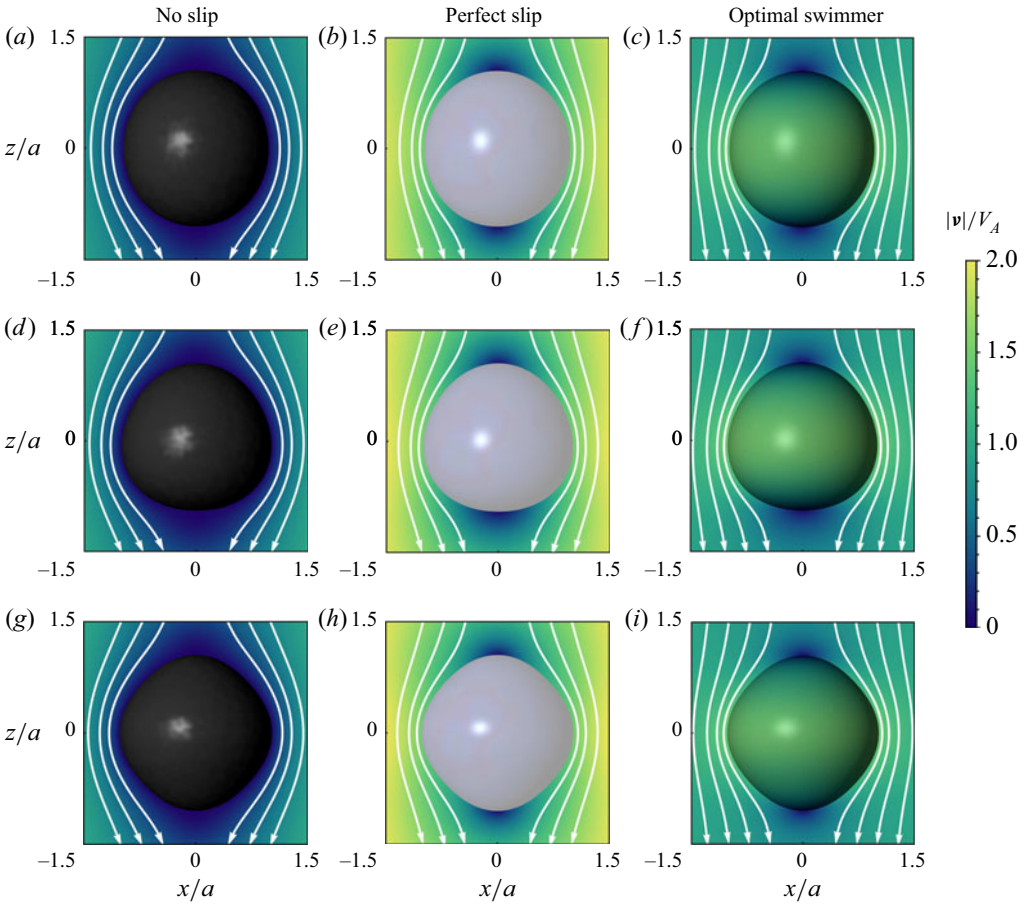


Figure 2. Streamlines around a slightly deformed sphere with no-slip (*a*,*d*,*g*), perfect-slip (*b*,*e*,*h*) and optimal active swimmer (*c*,*f*,*i*) in the co-moving frame. Each row shows one deformation mode with the amplitude $\alpha_\ell = 0.05$ for: $\ell = 2$ (*a–c*), $\ell = 3$ (*d–f*), and $\ell = 4$ (*g–i*). The colour indicates the fluid velocity, scaled by the speed of the active swimmer.

A Taylor expansion up to linear order in $\alpha_\ell$ leads to

$$v_r^{(0)} + \alpha_\ell \left( v_r^{(1)} + v_\theta^{(0)} P_\ell^1(\cos\theta) + a \frac{\partial v_r^{(0)}}{\partial r} P_\ell(\cos\theta) \right) \Bigg|_{r=a} = 0, \tag{3.7a}$$

$$\sigma_{r\theta}^{(0)} + \alpha_\ell \left( \sigma_{r\theta}^{(1)} + \left( \sigma_{rr}^{(0)} - \sigma_{\theta\theta}^{(0)} \right) P_\ell^1(\cos\theta) + a \frac{\partial \sigma_{r\theta}^{(0)}}{\partial r} P_\ell(\cos\theta) \right) \Bigg|_{r=a} = 0. \tag{3.7b}$$

Again, we solve the flow problem using Lamb's solution (3.3) and determine the coefficients $A_n$ and $B_n$ that satisfy the above conditions. The solution for the zeroth-order problem corresponding to an undeformed sphere is obtained by requiring $v_r^{(0)} = 0$ and $\sigma_{r\theta}^{(0)} = 0$, which readily leads us to $A_1^{(0)} = 1$, $B_1^{(0)} = 0$ and $A_n^{(0)} = B_n^{(0)} = 0$ for $n \geqslant 2$. Thus, at the zeroth order we have

$$\frac{v_r^{(0)}}{V_{PS}} = -\left(1 - \frac{a}{r}\right)\cos\theta, \quad \frac{v_\theta^{(0)}}{V_{PS}} = \frac{1}{2}\left(2 - \frac{a}{r}\right)\sin\theta \tag{3.8a,b}$$

which, as expected, is the flow past a spherical air bubble (Happel & Brenner 1983).

Proceeding to the first order, noting that $\sigma^{(0)}_{r\theta} = \sigma^{(0)}_{\theta\theta} = 0$ everywhere in the fluid domain, we again find that all the terms except $n = \ell \pm 1$ are zero. The first-order coefficients arising from the effect of $\alpha_\ell$ are thereby found as

$$A^{(1)}_{\ell-1} = -\frac{(\ell+1)(\ell+2)}{(2\ell-1)(2\ell+1)}, \quad A^{(1)}_{\ell+1} = \frac{\ell^2+\ell+3}{(2\ell+3)(2\ell+1)}, \tag{3.9a}$$

$$B^{(1)}_{\ell-1} = -\frac{(\ell-1)(\ell^2+\ell+3)}{2(2\ell-1)(2\ell+1)}, \quad B^{(1)}_{\ell+1} = \frac{\ell(\ell-1)(\ell+1)}{2(2\ell+3)(2\ell+1)}. \tag{3.9b}$$

These coefficients determine the first-order solution for the flow field with the perfect-slip boundary condition (figure 2*b*,*e*,*h*). From the drag force $F_D = -4\pi\mu a A_1 V_{PS}$, we determine the drag coefficient as

$$\frac{R_{PS}}{4\pi\mu a} = 1 - \frac{4}{5}\alpha_2. \tag{3.10}$$

The result is consistent with the calculation for an ellipsoidal particle, where only the deformation mode $\ell = 2$ is present (Chang & Keh 2009), but has a broader validity, as it shows that deformation modes beyond the second do not influence the drag coefficient in linear order.

## 4. Optimal active swimmer

Having derived the solutions of the flow problems for no-slip and perfect-slip boundary conditions, we next make use of these solutions to construct the flow field induced by a self-propelling active microswimmer with minimum dissipation, i.e. the optimal swimmer. As shown in (2.3), the flow field surrounding the optimal swimmer can be reconstructed by a linear superposition of the flow fields of the no-slip and perfect-slip problems, weighted by a specific combination of their drag coefficients.

### 4.1. *Stresslet of the optimal microswimmer*

We first evaluate the stresslet of the optimal swimmer and its dipole coefficient. Because both passive flows are expanded in terms of Lamb's solution, their superposition, too, has the same form. A comparison between the flow field in (3.3) and the definition of the stresslet (2.2) shows that only the coefficient $A_2$ contributes to the stresslet. Specifically, the dipolar contribution to the flow field, which decays as $r^{-2}$, reads $\boldsymbol{v}/V = \frac{3}{2}A_2(3\cos^2\theta - 1)(a/r)^2\boldsymbol{e}_r$, which indicates that the dipole coefficient must be $\beta = -(3/2)A_2$. Note that $A^{(1)}_2 \neq 0$ only for $\ell \in \{1, 3\}$ and here we have set $\alpha_1 = 0$, so in the perturbative expansion the dipole coefficient evaluates to

$$\beta = -\frac{3}{2}\mathcal{A}^{(1)}_2\alpha_3, \tag{4.1}$$

with

$$\mathcal{A}^{(1)}_2 = \frac{R_{NS}}{R_{NS}-R_{PS}}\left[A^{(1)}_2\right]_{PS} - \frac{R_{PS}}{R_{NS}-R_{PS}}\left[A^{(1)}_2\right]_{NS} \tag{4.2}$$

being the corresponding coefficient of the active swimmer, expressed in terms of those of the NS and PS problems.

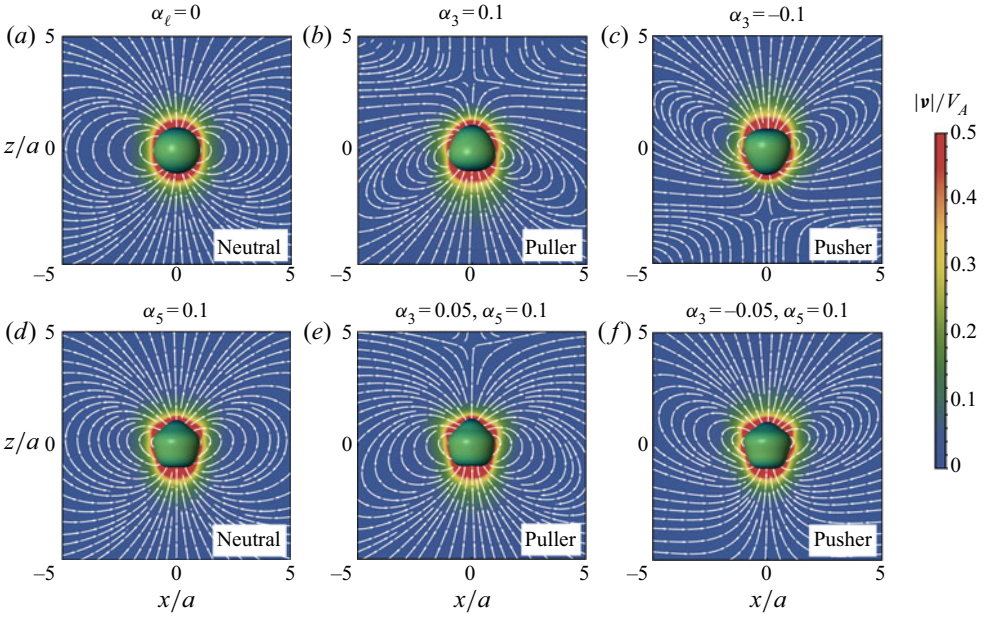


Figure 3. Streamlines in laboratory frame of optimal swimmers of various shapes. The non-zero surface modes for each swimmer are given at the top of each panel. The colours in the flow field indicate its velocity scaled by the swimming speed of the active particle. The swimmer surface colours represent the slip velocity as in figure 2.

From (4.1), one can see that the corrections to the drag coefficients $R_{NS}$ and $R_{PS}$ do not have any contributions to $\beta$ in the leading order. Equation (4.2) can therefore be evaluated with the drag coefficients of spherical particles. Remarkably, the dipole coefficient, to the leading order, only depends on the third Legendre mode of the shape function ($\alpha_3$), and other modes have no contribution. Inserting the values of $A_2^{(1)}$ from the NS and PS calculations into (4.1), we finally arrive at our final solution given in (2.4).

### 4.2. *Flow field of the optimal microswimmer*

The full velocity field induced by the optimal active microswimmer (figure 2*c*,*f*,*i*) can be obtained up to the linear order in deformation amplitudes by evaluating all coefficients in the same way as shown in (4.2). Thereby, the drag coefficients $R_{NS}$ and $R_{PS}$ need to be evaluated to linear order, as given in (3.5) and (3.10). In figure 3, the flow fields for some nearly spherical optimal swimmers are shown in the laboratory frame.

## 5. Conclusions

In this study we analysed the swimming type of nearly spherical optimal swimmers. We applied the minimum dissipation theorem (Nasouri *et al.* 2021) to determine the flow field of the optimal swimmer and to show that the dipole coefficient (or the strength of the stresslet) only depends to leading order on the third mode of the shape function. Thus, depending on the sign of this mode, the optimal swimmer is a puller (when positive), pusher (when negative) or neutral (when zero). Using our results, one can determine the optimal swimming type for surface-driven nearly spherical swimmers by simply describing the shape function in terms of the Legendre expansion and calculating the third

mode. Our results can also be applied to phoretic particles which use their surface activity to gain propulsion. For instance, for a chemically active particle, the slip velocity depends on the surface coating pattern which characterizes the chemical activity and mobility rates. For a given nearly spherical phoretic particle, one can then use our results to determine whether that surface coating minimizes the viscous dissipation. In the hydrodynamically optimal case, the dipole coefficient follows from the shape as derived here. We should note that for optimizing phoretic particles, one should also account for the dissipation in the slip layer and the energetics of the chemical reaction (Sabass & Seifert 2010, 2012), which is not considered here and can be a natural extension to this work.

Our derivation demonstrates how the recently proposed theorem can enable us to find a perturbative explicit solution to a problem that would otherwise hardly be analytically tractable. It is also possible to extend the presented results by accounting for the nonlinear effect of the quadratic and higher-order terms, in which case the contribution of other surface modes will be non-zero. Beyond that, one can use the methodology discussed here to evaluate the swimming type of any optimal swimmer of any arbitrary shape, provided the flow fields for the no-slip and perfect-slip problems are known.

**Funding.** This work was supported by the Deutsche Forschungsgemeinschaft (A.D.M.I., grant number DA 2107/1-1); Slovenian Research Agency (A.V., grant number P1-0099); and the Max Planck Society.

**Declaration of interests.** The authors report no conflicts of interest.

**Author ORCIDs.**
Abdallah Daddi-Moussa-Ider https://orcid.org/0000-0002-1281-9836;
Babak Nasouri https://orcid.org/0000-0002-4376-2510;
Andrej Vilfan https://orcid.org/0000-0001-8985-6072;
Ramin Golestanian https://orcid.org/0000-0002-3149-4002.

## References

Alouges, F., DeSimone, A. & Lefebvre, A. 2007 Optimal strokes for low Reynolds number swimmers: an example. *J. Nonlinear Sci.* **18**, 277–302.

Batchelor, G.K. 1970 The stress system in a suspension of force-free particles. *J. Fluid Mech.* **41**, 545–570.

Bechinger, C., Di Leonardo, R., Löwen, H., Reichhardt, C., Volpe, G. & Volpe, G. 2016 Active particles in complex and crowded environments. *Rev. Mod. Phys.* **88**, 045006.

Berke, A.P., Turner, L., Berg, H.C. & Lauga, E. 2008 Hydrodynamic attraction of swimming microorganisms by surfaces. *Phys. Rev. Lett.* **101**, 038102.

Blake, J. 1973 A finite model for ciliated micro-organisms. *J. Biomech.* **6**, 133–140.

Blake, J.R. 1971 A spherical envelope approach to ciliary propulsion. *J. Fluid Mech.* **46**, 199–208.

Blake, J.R. & Sleigh, M.A. 1974 Mechanics of ciliary locomotion. *Biol. Rev.* **49**, 85–125.

Chang, Y.C. & Keh, H.J. 2009 Translation and rotation of slightly deformed colloidal spheres experiencing slip. *J. Colloid Interface Sci.* **330**, 201–210.

Daddi-Moussa-Ider, A., Lisicki, M., Mathijssen, A.J.T.M., Hoell, C., Goh, S., Bławzdziewicz, J., Menzel, A.M. & Löwen, H. 2018 State diagram of a three-sphere microswimmer in a channel. *J. Phys.: Condens. Matter* **30**, 254004.

Drescher, K., Leptos, K.C., Tuval, I., Ishikawa, T., Pedley, T.J. & Goldstein, R.E. 2009 Dancing *Volvox*: hydrodynamic bound states of swimming algae. *Phys. Rev. Lett.* **102**, 168101.

Golestanian, R., Liverpool, T.B. & Ajdari, A. 2005 Propulsion of a molecular machine by asymmetric distribution of reaction products. *Phys. Rev. Lett.* **94**, 220801.

Gompper, G., Winkler, R.G., Speck, T., Solon, A., Nardini, C., Peruani, F., Löwen, H., Golestanian, R., Kaupp, U.B., Alvarez, L., *et al.*2020 The 2020 motile active matter roadmap. *J. Phys.: Condens. Matter* **32**, 193001.

Guo, H., Zhu, H., Liu, R., Bonnet, M. & Veerapaneni, S. 2021 Optimal slip velocities of micro-swimmers with arbitrary axisymmetric shapes. *J. Fluid Mech.* **910**, A26.

Happel, J. & Brenner, H. 1983 *Low Reynolds Number Hydrodynamics*. Martinus Nijhoff.

ITO, H., OMORI, T. & ISHIKAWA, T. 2019 Swimming mediated by ciliary beating: comparison with a squirmer model. *J. Fluid Mech.* **874**, 774–796.
KANTSLER, V., DUNKEL, J., POLIN, M. & GOLDSTEIN, R.E. 2013 Ciliary contact interactions dominate surface scattering of swimming eukaryotes. *Proc. Natl Acad. Sci. USA* **110**, 1187–1192.
KELLER, S.R. & WU, T.Y. 1977 A porous prolate-spheroidal model for ciliated micro-organisms. *J. Fluid Mech.* **80**, 259–278.
KIM, S. & KARRILA, J.S. 1991 *Microhydrodynamics: Principles and Selected Applications*. Butterworth-Heinemann.
LAUGA, E. & ELOY, C. 2013 Shape of optimal active flagella. *J. Fluid Mech.* **730**, R1.
LAUGA, E. & MICHELIN, S. 2016 Stresslets induced by active swimmers. *Phys. Rev. Lett.* **117**, 148001.
LAUGA, E. & POWERS, T.R. 2009 The hydrodynamics of swimming microorganisms. *Rep. Prog. Phys.* **72**, 096601.
LIGHTHILL, J. 1975 *Mathematical Biofluiddynamics*. Society for Industrial and Applied Mathematics.
LIGHTHILL, M.J. 1952 On the squirming motion of nearly spherical deformable bodies through liquids at very small Reynolds numbers. *Commun. Pure Appl. Maths* **5**, 109–118.
LIN, Z., THIFFEAULT, J.-L. & CHILDRESS, S. 2011 Stirring by squirmers. *J. Fluid Mech.* **669**, 167–177.
MICHELIN, S. & LAUGA, E. 2010 Efficiency optimization and symmetry-breaking in a model of ciliary locomotion. *Phys. Fluids* **22**, 111901.
NASOURI, B. & ELFRING, G.J. 2018 Higher-order force moments of active particles. *Phys. Rev. Fluids* **3**, 044101.
NASOURI, B. & GOLESTANIAN, R. 2020 Exact phoretic interaction of two chemically active particles. *Phys. Rev. Lett.* **124**, 168003.
NASOURI, B., VILFAN, A. & GOLESTANIAN, R. 2019 Efficiency limits of the three-sphere swimmer. *Phys. Rev. Fluids* **4**, 073101.
NASOURI, B., VILFAN, A. & GOLESTANIAN, R. 2021 Minimum dissipation theorem for microswimmers. *Phys. Rev. Lett.* **126**, 034503.
OMORI, T., ITO, H. & ISHIKAWA, T. 2020 Swimming microorganisms acquire optimal efficiency with multiple cilia. *Proc. Natl Acad. Sci. USA* **117**, 30201–30207.
OSTERMAN, N. & VILFAN, A. 2011 Finding the ciliary beating pattern with optimal efficiency. *Proc. Natl Acad. Sci. USA* **108**, 15727–15732.
PEDLEY, T.J., BRUMLEY, D.R. & GOLDSTEIN, R.E. 2016 Squirmers with swirl: a model for Volvox swimming. *J. Fluid Mech.* **798**, 165–186.
PIRONNEAU, O. & KATZ, D.F. 1974 Optimal swimming of flagellated micro-organisms. *J. Fluid Mech.* **66**, 391–415.
SABASS, B. & SEIFERT, U. 2010 Efficiency of surface-driven motion: nanoswimmers beat microswimmers. *Phys. Rev. Lett.* **105**, 218103.
SABASS, B. & SEIFERT, U. 2012 Dynamics and efficiency of a self-propelled, diffusiophoretic swimmer. *J. Chem. Phys.* **136**, 064508.
SHAPERE, A. & WILCZEK, F. 1987 Self-propulsion at low Reynolds number. *Phys. Rev. Lett.* **58**, 2051–2054.
SHAPERE, A. & WILCZEK, F. 1989 Efficiencies of self-propulsion at low Reynolds number. *J. Fluid Mech.* **198**, 587–599.
SPAGNOLIE, S.E., MORENO-FLORES, G.R., BARTOLO, D. & LAUGA, E. 2015 Geometric capture and escape of a microswimmer colliding with an obstacle. *Soft Matt.* **11**, 3396–3411.
SPRENGER, A.R., SHAIK, V.A., ARDEKANI, A.M., LISICKI, M., MATHIJSSEN, A.J.T.M., GUZMÁN-LASTRA, F., LÖWEN, H., MENZEL, A.M. & DADDI-MOUSSA-IDER, A. 2020 Towards an analytical description of active microswimmers in clean and in surfactant-covered drops. *Eur. Phys. J.* E **43**, 58.
STONE, H.A. & SAMUEL, A.D.T. 1996 Propulsion of microorganisms by surface distortions. *Phys. Rev. Lett.* **77**, 4102–4104.
UNDERHILL, P.T., HERNANDEZ-ORTIZ, J.P. & GRAHAM, M.D. 2008 Diffusion and spatial correlations in suspensions of swimming particles. *Phys. Rev. Lett.* **100**, 248101.
VILFAN, A. 2012 Optimal shapes of surface slip driven self-propelled microswimmers. *Phys. Rev. Lett.* **109**, 128105.
ZHANG, P., JANA, S., GIARRA, M., VLACHOS, P. & JUNG, S. 2015 Paramecia swimming in viscous flow. *Eur. Phys. J.: Spec. Top.* **224**, 3199–3210.